Ceramics International **21** (1995) 131–136

Laser Clad ZrO_2–Y_2O_3 Ceramic/Ni-base Alloy Composite Coatings

Y. T. Pei, J. H. Ouyang, T. C. Lei & Y. Zhou

Department of Metals and Technology, Harbin Institute of Technology, Harbin 150001, China

(Received 26 January 1994; accepted 9 March 1994)

Abstract: A laser cladding technique was used to produce ZrO_2–Y_2O_3 ceramic/Ni-base alloy composite coatings on stainless steel 4Cr13. The microstructure and hardness of the composite coatings are analyzed by XRD, SEM, EPMA, TEM and microhardness testing techniques. A stratification is observed in the laser clad zone. The upper region of the clad is a pure ZrO_2 ceramic layer, and the lower region is an excellent transition layer of Ni-base alloy. The ZrO_2 ceramic layer exhibits equiaxed grains and columnar structure of t' phase and a tiny network structure of m phase along the t' boundaries. The transition layer of Ni-base alloy shows the multi-phase structure of primary γ–Ni dendrites and dendritic eutectic, at interdendritic regions, of $(Fe, Cr)_{23}C_6$ carbide plus γ–Ni phase.

1 INTRODUCTION

Oxide ceramics are becoming increasingly important as an industrial material for their excellent properties such as heat, corrosion and wear resistance, chemical stability at high temperature, etc. Many investigators have reported that thermal spraying techniques can be used to produce ceramic deposits on different metallic substrates to enhance the surface properties of materials, especially for the use as thermal barrier coating.[1–3] However, the commonly existing porosity in the deposits and its weak adhesion to the substrate formed by thermal spraying reduce the effectiveness of the deposit. An approach to solve this problem is laser sealing of sprayed ceramic deposits.[4,5] By melting a thin layer of as-sprayed ceramics, fine microstructure together with non-porous and smooth layers can finally be obtained.

In the present work, a single laser cladding technique has been employed to produce a ZrO_2–Y_2O_3 ceramic/Ni-base alloy composite coating on stainless steel 4Cr13. The microstructure and hardness of the composite coating are analyzed, and the effect of laser processing parameters is discussed.

2 EXPERIMENTAL PROCEDURE

The 40 × 20 × 10 mm strips of hot rolled martensitic stainless steel 4Cr13 were used as the substrate with the chemical composition (wt%): 0·41C, 0·58Si, 0·76Mn, 13·2Cr. The clad material was a particulate mixture of 60 vol% yttria partially stabilized zirconia (YPSZ with 4 mol% Y_2O_3) and 40 vol% Ni-base self-fluxing alloy. The YPSZ powders have a particle size in the range from 0·05 to 1·0 μm. The chemical composition of the Ni-base self-fluxing alloy powders with an average particle size of 30 μm is (wt%): 15·0Cr, 4·05B, 5·88Si, 0·73C, 12·28Fe and Ni in balance.

A 2kW continuous wave CO_2 laser was employed to form single clad tracks from the powder mixture 0·5 mm thick preplaced on the substrate. The laser processing parameters used in the present investigation are D(beam diameter) = 3 mm, P(power) = 500–800W and V(scanning speed) = 2–10 mm/s. Argon gas was blown to keep the clad region separate from the atmosphere.

Transverse sections were cut for making measurements of the track dimensions. Microstructure and hardness analyses were done by SEM, EPMA and microhardness testing technique. Hot

Ceramics International. 0272-8842/95/$9.50

hydrofluoric acid and 1 mol% caustic soda electrolyte were employed to etch the ceramic layer and Ni-base alloy fusion layer, respectively. The phases in the initial powder and the laser clad layers were identified using X-ray diffraction with Cu Kα radiation. A step scanning mode was used for more detailed investigation of the phases with a 0·01 2θ step over the low 2θ ranges of 27–32° for the monoclinic (m) ($\bar{1}11$) and (111) peaks, the cubic (c), tetragonal (t), and non-transformable tetragonal (t') (111) peaks, as well as the high 2θ ranges between 72 and 76° for the t, t' (004) peaks and c, t, t' (400) peaks. The X-ray examination was carried out on the upper surface of the clads without grinding and polishing in order to prevent mechanically induced phase transformation.

3 RESULTS AND DISCUSSION

3.1 Phase analysis of the coating

Figure 1 compares the X-ray step scanning results for the initial YPSZ powder and the laser clad YPSZ ceramic composite coating. The XRD data for the initial YPSZ powder show the presence of t, m and c phases. In the clad composite coating, small peaks corresponding to the ($\bar{1}11$) and (111) reflections of the m phase are still evident in the low 2θ range (27–32°). However, only the (004) and (400) t' peaks are observed in the high 2θ range (72-76°). In addition, no peak corresponding to γ-Ni or any other nickel compound phase can be detected at any angle. This means that the upper surface layer of the clad coating consists of pure YPSZ ceramic. The contents of all phases are shown in Table 1.

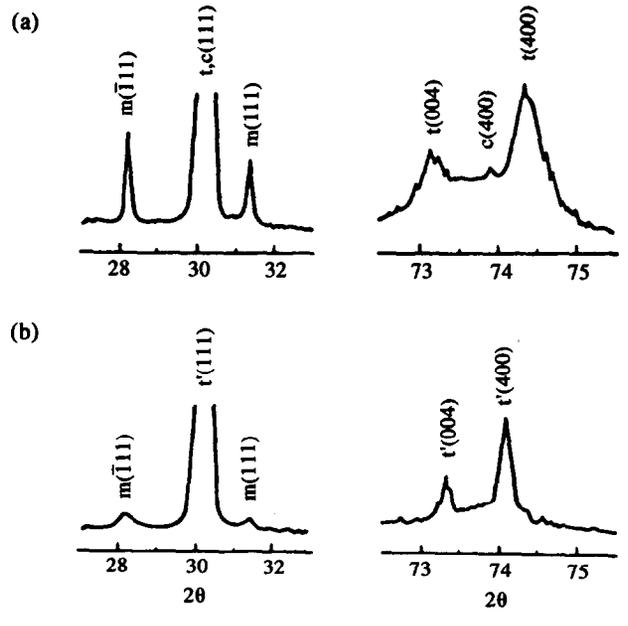

Fig. 1. XRD profiles for 4 mol% YPSZ initial powder (a) and laser clad layer (b).

Table 1. Phase content in 4 mol% YPSZ ceramics

Material	Phases (wt%)			
	t	m	c	t'
Initial powder	67·1	30·6	2·3	0
Laser clad layer	0	1·9	0	98·1

The coexistance of t, m and c phases in the initial YPSZ powders (Fig. 1(a)) indicates that the chemical composition of the powders is not uniform since the Y_2O_3 content increases in the sequence m→t→c. After laser cladding, the chemical composition of YPSZ becomes uniform upon melting and transforms from c to t' phase by a diffusionless mechanism upon rapid cooling after cladding. Such a diffusionless and displacive c–t transformation in ZrO_2-base ceramics with 5–12 wt% (about 3–7 mol%) Y_2O_3 was first reported by Scott.[6] This kind of transformation is referred to as the c–t' transformation because the substructure of t'-ZrO_2 product differs from that of the t-ZrO_2 phase. The previous investigations indicated that the t' phase does not transform on annealing at 1200°C for a long time,[7–9] which is of importance in relation to the service behaviour of thermal barrier coatings.

3.2 Aspect feature of the coating

The aspect features of the laser clad single tracks are mainly correlated to the specific energy. Figure 2 shows the relationship between the aspect ratio (W/H) of the composite coating and the specific energy. The aspect ratio is reduced with an increase in the specific energy.

3.3 Stratification feature of the coating

Figure 3 shows the cross-section of the composite coating. The cladding can be divided into two distinct regions. The upper region is a pure ZrO_2 layer about 200 μm thick, and the lower region is

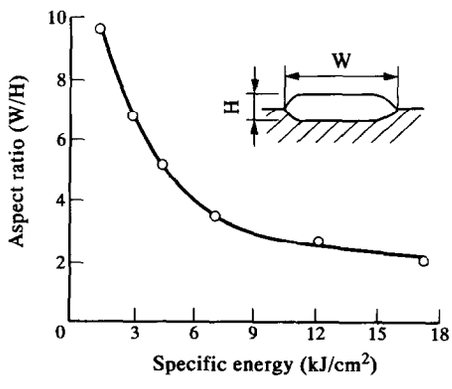

Fig. 2. Effect of specific energy on aspect ratio of the coating.

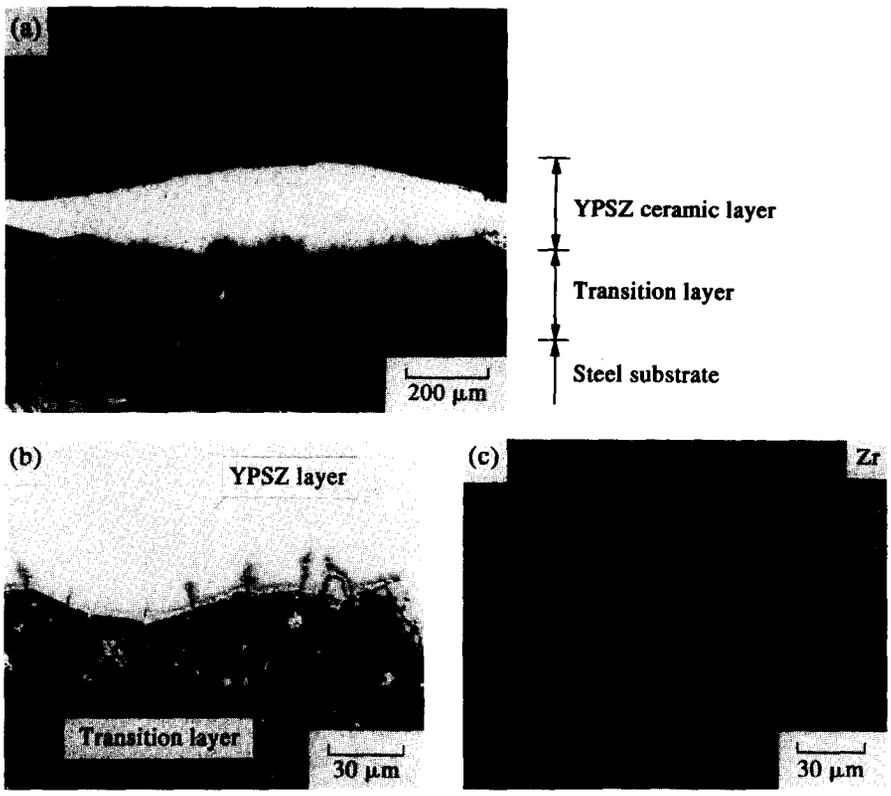

Fig. 3. Cross-section of the laser clad composite coating (D = 3 mm, P = 800 W and V = 8 mm/s): (a) general feature of the composite coating; (b) detail of the interfacial bonding between the ceramics and Ni-base transition layer; (c) distribution of Zr in the same field as in (b).

an excellent transition layer composed of the Ni-base alloy and the steel substrate. The thickness of the transition layer, ranging from 0·15 to 0·35 mm, depends on its dilution by the substrate elements associated with the laser processing parameters.

After the cladding of two kinds of powders, a stratification is observed in the coating. It is considered that complete melting of both the ceramics and the alloy had occurred during laser radiation and that there was some redistribution of components because of the difference of mass density and interfacial tension between two liquid phases, boosted by drastic convection in the molten pool.

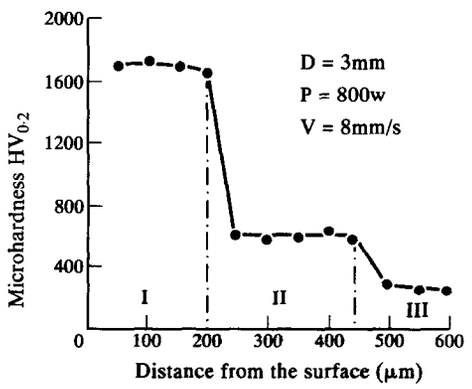

Fig. 4. Hardness of the composite coating examined on transverse sections; (I) ceramic layer, (II) transition layer, (III) steel substrate.

The melting temperature of the ceramics is of the order of 2750°C and is much higher than that of the Ni-base alloy, so that the ceramic solidifies first on the basis of immiscible liquids. This duplex structure is of importance for the composite coating to give full use of the advantageous properties of ceramics in the upper region as an ideal protecting layer. On the other hand, the transition layer of Ni-base alloy is able to relax the abrupt changes of the physical and mechanical properties between the ceramics and the substrate.

The microhardness distribution shown in Fig. 4 clearly exhibits three steps corresponding to the upper ceramic layer, the transition layer of the Ni-base alloy and the substrate, respectively. The hardness of the clad ceramics has a maximum value of $HV_{0.2}$ = 1720 and is almost constant in the whole region, which illustrates that the ceramic layer is homogeneous and dense.

3.4 Microstructure of the composite coating

In Fig. 5 it is shown that the ceramic layer exhibits equiaxed grains and a columnar structure of t' phase at the upper and the middle-bottom regions of the ceramic layer, respectively. A tiny network of 'dark' phase is distributed along the t' boundary and is attributed to m-ZrO_2 phase formed from the metastable t phase on cooling.

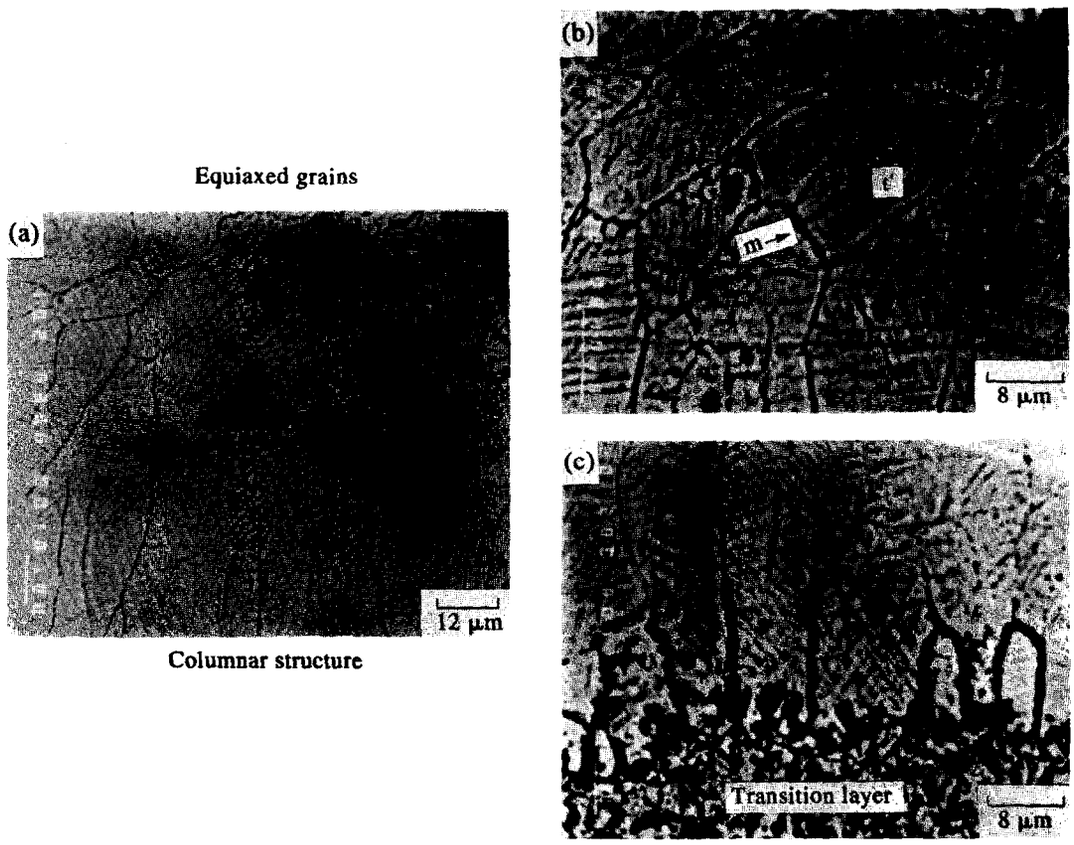

Fig. 5. SEM images showing the microstructure of laser clad YPSZ ceramic layer (D = 3 mm, P = 800 W and V = 8 mm/s: (a) general feature of the ceramic layer; (b) BEI image showing t' equiaxed grains and tiny network of m-phase at the top regions of the ceramic layer; (c) columnar structure of t'-phase at the bottom regions of the ceramic layer.

Such a distribution of m-phase is consistent with yttria depletion at the boundary. In addition, a lamellar substructure can be seen within the t' phase grains and is probably correlated with the domain and twinned microstructure of the t'-ZrO_2 phase reported earlier.[10–12]

Within the ceramic layer, about 15 μm thick over the transition layer, the interspaces between t' columnar grains are filled with γ-Ni solid solution (Figs 5(c) and 3(b)). Figure 6 shows the line scanning results of phase composition through the interface region. These γ-Ni roots can increase significantly the bonding strength between the ceramic layer and the steel substrate. Moreover, such a structure can help to form a 'buffer' in order to relax the thermal stress throughout the bonding region.

The transition layer of Ni-base alloy shows primary dendrites of γ-Ni solid solution and eutectics at intergranular spaces (Fig. 7). These dendrites nucleate from the bottom of the molten pool and grow upwards. The primary arm spacing of dendrites is about 5–8 μm depending on laser processing parameters. From Fig. 7(b), TEM examinations reveal that the dendritic eutectics consist of (Fe, $Cr)_{23}C_6$ carbide and Ni-base phase. The eutectic γ-Ni phase differs from the primary γ-Ni

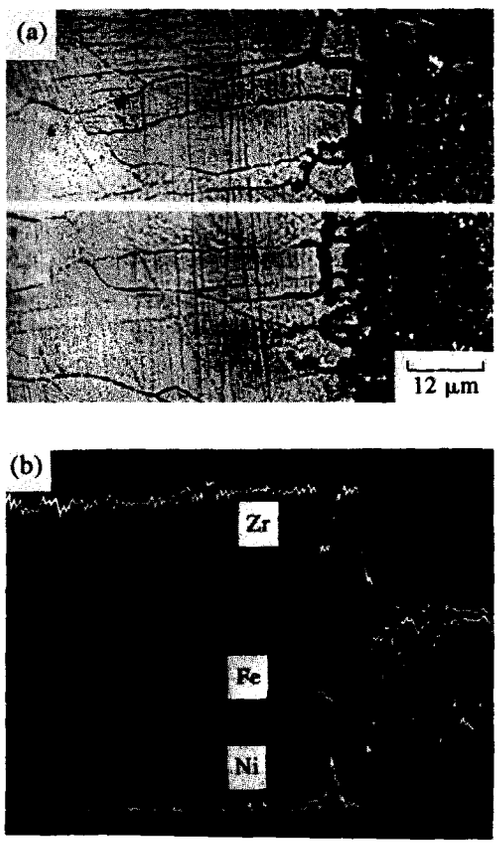

Fig. 6. EPMA line scanning analysis of phase composition through the interface region: (a) the location of scanning line; (b) Zr, Fe and Ni compositional profiles.

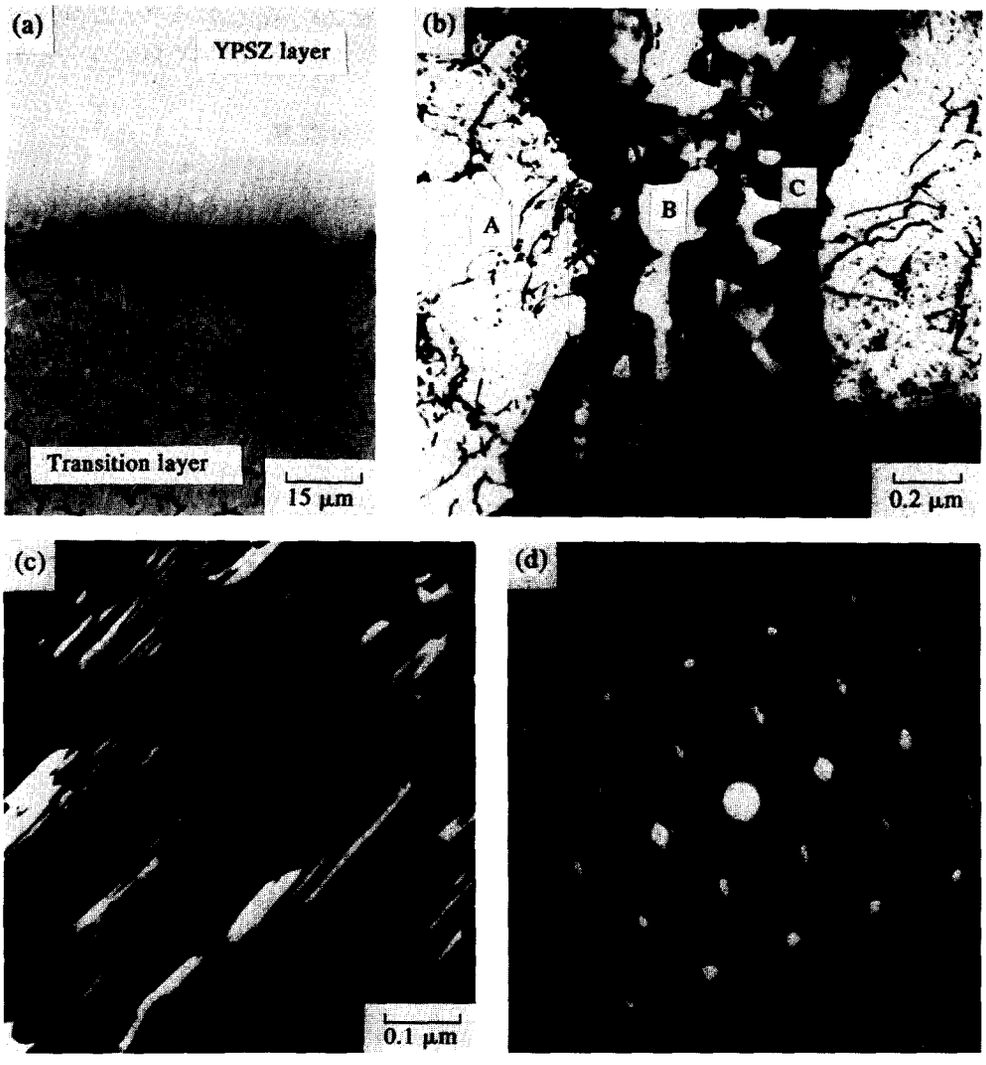

Fig. 7. Microstructure of the transition layer of Ni-base alloy (D = 3 mm, P = 800 W and V = 8 mm/s): (a) SEM image showing general features of the transition layer; (b) bright field TEM showing dense dislocation in primary γ-Ni phase and the eutectic of (Fe, Cr)$_{23}C_6$ carbide plus γ-Ni phase; (c) dark field TEM showing stacking-faults in the carbide phase; (d) synthetic diffraction pattern of the carbide and γ-Ni phase.

dendrite only in its chemical composition, and the former has higher Si and Ni contents but lower Cr and Fe contents confirmed by EDXA results (Table 2). This is attributed to the formation of the eutectic (Fe, Cr)$_{23}C_6$ carbide. Dense dislocations are observed within the primary γ-Ni dendrites, and stacking-faults within the carbide.

3.5 Hardness

Figure 8 shows the relationship between the hardness of the clad ceramic layer and the scanning speed. There is an optimum speed value at which the highest hardness of the ceramic layer can be obtained. If the scanning speed is too fast, the laser energy absorbed by the preplaced powders must be insufficient to melt both the YPSZ and alloy powders so that the clad is not dense and possesses a low hardness. But if the scanning

Table 2. EDXA results for carbide and γ phases in the transition layer

Measurement location	Phase	Composition (at%) Ni	Cr	Fe	Si
A	γ	38·4	18·5	42·8	4·3
B	γ	56·6	2·9	33·1	7·4
C	carbide	11·9	41·5	46·2	0·4

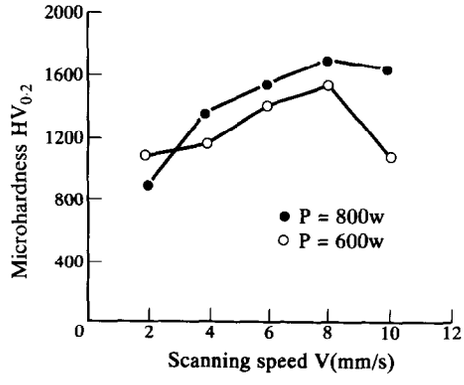

Fig. 8. Effect of scanning speed on the hardness of the clad YPSZ layer.

speed is too slow, the increase of interacting time between laser beam and powders causes a slow cooling rate together with an increase of m phase; therefore the hardness decreases slightly.

4 CONCLUSIONS

The following conclusions can be made:

(1) A stratification is observed in a laser clad ZrO_2–Y_2O_3 ceramic/Ni-base alloy composite coating, which contains two distinct regions; one is the upper layer of pure ZrO_2 ceramic and the other is an excellent transition layer composed of Ni-base alloy and the steel substrate.

(2) The ZrO_2 ceramic layer exhibits equiaxed grains and a columnar structure of t' phase and a tiny network structure of m-phase along the t' boundaries. Such a layer has a higher hardness value of $HV_{0.2}$ = 1720 and gives a high bonding strength with the substrate.

(3) The transition layer shows the multi-phase structure of primary γ-Ni dendrites and eutectics of $(Fe, Cr)_{23}C_6$ carbide plus γ-Ni phase.

REFERENCES

1. ASHARY, A. A. & TUCHER, Jr, R. C., *Surf. Coat. Technol.*, **49** (1991) 78–82.
2. PETITBON, A., BOQUET, L. & DELSART, D., *Mater. Sci. Eng.*, **A121** (1989). 545–48.
3. VIJANDE-DIAZ, R. *et al.*, *Wear* **148** (1991) 221–33.
4. IWAMOTO, N., UMESAKI, N., KATAYAMA, Y. & KUROKI, H., *Surf. Coat. Technol.*, **34** (1988) 59–67.
5. SMUROV, I., UGLOV, A., STURLESS, YU. & BARTULI, C., *J. Mater. Sci.*, **27** (1992) 4523–30.
6. SCOTT, H. G., *J. Mater. Sci.*, **10**(9) (1975) 1572–85.
7. WU, B. C., CHANG, E., CHANG, S. F. & TU, D., *J. Am. Ceram. Soc.*, **72**(2) (1989) 212–18.
8. BENNETT, A., *Mater. Sci. Technol.*, **2**(3) (1986) 257–61.
9. JASIM, K. M., RAWLINGS, R. D. & WEST, D. R. F., *Mater. Sci. Technol.*, **8** (1992) 83–91.
10. ZHOU, Y., LEI, T. C. & SAKUMA, T., *J. Am. Ceram. Soc.*, **74**(3) (1991) 633–40.
11. SAKUMA, T., *J. Mater. Sci.*, **22**(12) (1987) 4470–75.
12. CHAIM, R., RUHLE, M. & HEUER, A. H., *J. Am. Ceram. Soc.*, **68**(8) (1985) 427–31.